Enhanced Photosusceptibility near T_c for the Light-Induced Insulator-to-Metal Phase Transition in Vanadium Dioxide

D. J. Hilton,[1,*] R. P. Prasankumar,[1] S. Fourmaux,[2] A. Cavalleri,[3] D. Brassard,[2] M. A. El Khakani,[2] J. C. Kieffer,[2] A. J. Taylor,[1] and R. D. Averitt[1,†]

[1]*Center for Integrated Nanotechnologies, MS K771, Los Alamos National Laboratory, Los Alamos, New Mexico 87545, USA*
[2]*Université du Québec, INRS-Énergie et Matériaux et Télécommunications, Varennes, Québec, Canada J3X 1S2*
[3]*Department of Physics, Clarendon Laboratory, University of Oxford, Parks Road, Oxford, OX1 3PU, United Kingdom*

(Received 6 June 2006; published 30 November 2007)

We use optical-pump terahertz-probe spectroscopy to investigate the near-threshold behavior of the photoinduced insulator-to-metal (IM) transition in vanadium dioxide thin films. Upon approaching T_c a reduction in the fluence required to drive the IM transition is observed, consistent with a softening of the insulating state due to an increasing metallic volume fraction (below the percolation limit). This phase coexistence facilitates the growth of a homogeneous metallic conducting phase following superheating via photoexcitation. A simple dynamic model using Bruggeman effective medium theory describes the observed initial condition sensitivity.

DOI: 10.1103/PhysRevLett.99.226401 PACS numbers: 71.30.+h, 72.80.Ga, 78.47.+p

Strongly correlated electron materials are characterized by extreme sensitivity to external stimuli which results from the subtle interplay between many degrees of freedom with comparable energy scales (lattice, orbital, electronic, and magnetic). High temperature superconductivity, colossal magnetoresistance, exotic magnetic, charge, and orbital ordering, and insulator-to-metal (IM) transitions are some of the best known examples.

During the past several years, time-resolved optical studies have been utilized to investigate dynamics associated with the competing degrees of freedom in these materials [1]. In many of these studies the goal is to interrogate the dynamics within a particular phase. However, photoinduced phase transitions provide an important complementary approach to investigate the physical pathway connecting different correlated electron states as well as their mutual competition [2].

A photoinduced phase transition can arise following impulsive heating or photodoping and provides a means of controlling the overall phase of a solid on an ultrafast time scale [3–5]. One model system used to study insulator-to-metal transitions in correlated electron systems is vanadium dioxide (VO_2). This material undergoes an insulator-to-metal transition when heated above 340 K accompanied by a structural distortion from a monoclinic to a rutile phase [6–8]. Time-resolved optical studies can provide insight into its origin and its technological potential [9–11].

The interplay between band and Mott-insulating behavior in VO_2 has been addressed in the time domain, where a limiting structural time scale for the creation of the metallic phase suggests the importance of the atomic structural arrangements in determining the insulating state, i.e., reminiscent of a band insulator [12]. Advances in ultrafast technology have also enabled more comprehensive investigations involving, most recently, femtosecond x-ray absorption spectroscopy [13,14].

In this Letter, we measure the time-dependent conductivity of VO_2 during a photoinduced insulator-to-metal transition. Our dynamic experiments focus on the poorly understood near-threshold behavior, where phase separation and domain formation inhibit the measurement of conventional transport properties since a macroscopic conductivity pathway is not established [15]. As a function of increasing initial temperature (up to $\sim T_c$) we observe a reduction in the deposited energy required to drive the IM transition. Such a response indicates an initial condition sensitivity which we interpret as a softening of the insulating state due to the existence of metallic precursors. These precursors facilitate the growth of a homogeneous metallic conducting phase following superheating. A simple dynamic model using Bruggeman effective medium theory describes the observed response. We emphasize that this percolation model is valid near threshold whereas, at higher fluences, the transition is prompt and nonthermal [12–14]. Our results may be relevant in other systems which exhibit tendencies toward phase separation such as spin-crossover complexes [16].

Our (011) oriented VO_2 thin film was grown on a (100) MgO substrate by radio-frequency (13.56 MHz) magnetron sputtering of a vanadium target (99.99% purity) in an Ar and O_2 mixture at a pressure of 2 mTorr (chamber base pressure of 2×10^{-8} Torr) and a temperature of 500 °C [17]. The stability of the deposition process and the thickness of the films (100 nm) were monitored *in situ* by a calibrated microbalance and independently verified using standard ellipsometric techniques. The crystalline quality, grain size, and orientation of the VO_2 films were characterized by x-ray diffraction.

First, we determined the time-independent THz conductivity of our VO_2 films as a function of sample temperature. We use the output of a 50 fs titanium:sapphire amplifier to generate nearly single-cycle THz pulses via optical recti-

fication in ZnTe and employ standard terahertz time-domain spectrometry to measure the THz frequency conductivity; further details can be found in Refs. [18,19]. In Fig. 1(a), we show the transmitted THz waveform at 340 K, where the top waveform (displaced for clarity) results when the sample is heated from 300 to 340 K and the bottom results when the sample is cooled from 370 to 340 K. From the time-domain data, the calculated conductivity of the VO_2 film from 0.25 THz to 2.25 THz is determined [Fig. 1(b)].

Figure 1(c) shows the magnitude of the real conductivity as a function of temperature. We also plot the temperature-dependent dc electrical conductance measured (on the same film) between two metal contacts, which shows good agreement with the temperature dependence of the THz conductivity. The hysteresis is consistent with the first order phase transition in VO_2 and the narrow width (<5 K) and magnitude of the metallic state conductivity attest to the quality of our films [6,20].

In order to study the conductivity dynamics of the photoinduced phase transition, we excite the sample using 1.55 eV pulses from the amplified laser and monitor the change in the THz transmission as a function of the relative delay between the pump pulse and the THz-probe pulse [1]. This film is approximately one optical absorption length thick at 800 nm, which results in a nonuniform excitation profile along the direction of propagation; however, this does not significantly influence our results. We have verified that the induced change in conductivity is frequency independent across the bandwidth of our THz pulse indicating uniform excitation across the THz-probe beam.

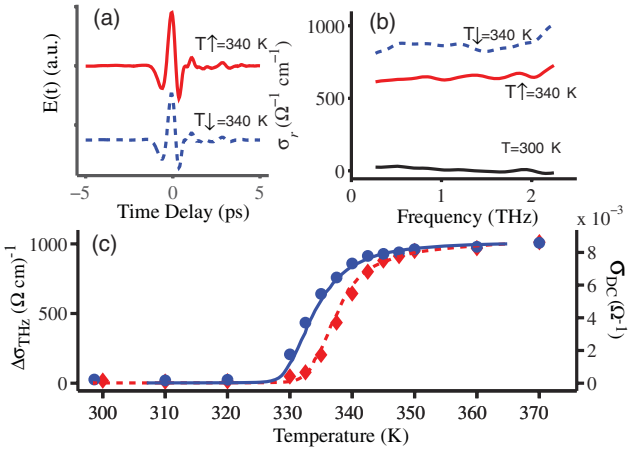

FIG. 1 (color online). (a) THz waveform transmitted through the sample when heated to 340 from 300 K ($T_\uparrow$) and when cooled from 370 K ($T_\downarrow$), offset for clarity. (b) The optical conductivity vs frequency as determined from the transmitted waveforms in (a) and at 300 K. (c) The temperature-dependent hysteresis of the THz conductivity (left scale, ◆ for $T_\uparrow$, ● for $T_\downarrow$) and of the conductance measured using standard dc electrical techniques (right scale: dashed line for $T_\uparrow$; solid line for $T_\downarrow$).

Figure 2(a) shows the time-resolved conductivity as a function of pump fluence at 300 K. There is a rise time of $\sim$100 ps to obtain the conductivity of the product metallic phase at all fluences. This is significantly longer than the initial excitation pulse, meaning that photoconductivity arising from carriers excited to the conduction band (e.g., as occurs in GaAs) is not responsible for the induced response. Additionally, lattice heating via carrier thermalization occurs in approximately one picosecond indicating that the conductivity dynamics are more complex than simple heating above T_c. Crucially, however, for fluences greater than $\sim$10 mJ cm^{-2}, the deposited energy density ($\sim$500 J cm^{-3}) is considerably above what is required to heat above T_c ($\sim$200 J cm^{-3} at 300 K).

Figure 2(b) shows the maximum induced conductivity, $\Delta\sigma_{\max}$, at each pump fluence extracted from the data in Fig. 2(a). There is a marked decrease in the maximum obtainable conductivity with decreasing fluence. At a fluence of 19.2 mJ cm^{-2}, the induced conductivity at long times is 100% of the metallic phase conductivity (i.e., at 370 K). Extrapolation of the photoinduced conductivity change at 300 K, as shown in Fig. 2(b), yields a nonzero fluence threshold of $\sim$7 mJ cm^{-2}. The existence of a fluence threshold is a well-known feature in photoinduced phase transitions, where the cooperative nature of the dynamics results in a strongly nonlinear conversion efficiency as a function of the number of absorbed photons. In the present case, photoexcitation leads to a rapid increase of the lattice temperature, initiating the nucleation and growth of metallic domains which coalesce (i.e., percolate) to yield a macroscopic conductivity response.

We have also measured the photoinduced terahertz conductivity as a function of base temperature. An optical pump fluence of 12.8 mJ cm^{-2} was used, less than is

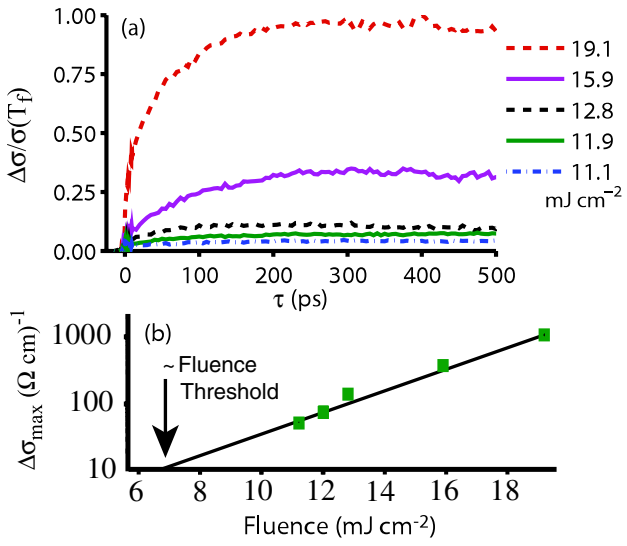

FIG. 2 (color online). (a) Photoinduced conductivity change at 300 K for various fluences where $\sigma(T_f)$ is the conductivity in the full metallic state. (b) Magnitude of the conductivity change as a function of fluence at 300 K.

required to drive the full metallic transition at room temperature (though, as described above, more than enough to superheat the film above T_c). The conductivity dynamics as a function of time at initial temperatures of 300, 310, and 320 K are displayed in Fig. 3(a). From Figs. 3(a) and 3(b) it is evident that, below T_c, the photoinduced change in the conductivity is less than the maximum possible induced change. However, with increasing initial temperature the induced conductivity change increases and obtains the maximum possible value at 320 K. Thus, in the insulating phase, there is a decrease in the threshold to drive the sample metallic with increasing temperature. At temperatures greater than 330 K, the photoinduced change in conductivity follows the maximum possible induced change [Fig. 3(b)]. This occurs since the incident fluence of 12.8 mJ cm^{-2} is sufficient to drive the conductivity to its full metallic state consistent with a decreasing threshold. Finally, in Fig. 3(c) we plot the fluence threshold as a function of base temperature as determined from several series of data such as that in Fig. 2(b). This further emphasizes the softening that occurs in the insulating state with increasing base temperature.

Summarizing the dynamics in Figs. 2 and 3, (i) the conductivity rise time of ~100 ps is substantially longer than the excitation pulse or electron thermalization time, (ii) a fluence of 12.8 mJ cm^{-2} heats the sample well in excess of T_c, (iii) despite (ii), the maximum possible conductivity is not obtained at 300 K, indicating a stiffness with respect to driving the IM transition and, (iv) this stiffness toward fully driving the IM transition decreases with increasing temperature indicating a softening of the insulating phase. While a complete description of the dynamics is difficult, in the following we present a simple dynamic model using Bruggeman effective medium theory that, to first order, describes the experimentally measured dynamics.

Bruggeman effective medium theory (BEMT) [21,22] is a mean field description to describe inhomogeneous media. For VO_2, this corresponds to the coexistence of a metallic volume fraction (f_m) and an insulating volume fraction ($1 - f_m$) which depend on temperature. Previous work has described the temperature-dependent conductivity (both the finite transition temperature width and hysteresis) in terms of the coexistence of metallic and insulating phases in VO_2 [6]. More recently, additional experimental support for this idea from time-integrated optical conductivity and scanning probe measurements has been presented [23,24].

BEMT describes the conductivity as follows:

$$f_m \frac{\sigma_m - \sigma_{\text{eff}}}{\sigma_m + (d-1)\sigma_{\text{eff}}} + (1 - f_m) \frac{\sigma_i - \sigma_{\text{eff}}}{\sigma_i + (d-1)\sigma_{\text{eff}}} = 0, \tag{1}$$

where σ_m is the conductivity in the metallic phase (1000 Ω^{-1} cm^{-1}) and $\sigma_i = 0$ is the conductivity in the insulating phase. As with previous descriptions of VO_2 using BEMT, we take the two-dimensional form ($d = 2$) of this expression ([23]). In this simple model, there exist disconnected metallic domains in the insulating phase. Percolation of the metallic domains occurs at $f_m = 0.50$, at which point the sample becomes conducting.

We can calculate the metallic volume fraction, f_m, using Eq. (1) and the experimental results presented in Fig. 1(c) for temperatures above T_c (◆ for $T_\uparrow$ and ● for $T_\downarrow$), which we plot in Fig. 4. The increasing temperature branch of the metallic fraction, $f_m(T_\uparrow)$, increases from 0.52 at 330 K to 0.98 at 350 K, while the decreasing temperature branch, $f_m(T_\downarrow)$, returns to 0.61 at 330 K, a consequence of the conductivity hysteresis exhibited in this material. In the insulating phase, we cannot use this approach to determine f_m since the conductivity is below our detection limit.

To describe the conductivity dynamics in the insulating phase using BEMT we determine the temporal dependence of the volume fraction using the following expression:

$$\frac{df_m}{dt} = f_m(1 - f_m)\beta(T). \tag{2}$$

With this simple model, the growth rate of f_m depends on directly on f_m, the available nonmetallic fraction $(1 - f_m)$, and $\beta(T)$ which describes the rate at which f_m evolves. It is reasonable to assume $\beta(T) = \beta_0 \exp(-\Theta/k_b T)$ which describes an Arrhenius-like temperature dependence where Θ is an energy barrier related, in the present case, to the latent heat. For example, for homogeneous domain growth, $\Theta \propto (T - T_c)^{-2}$ [25]. The temperature dependence of $\beta(T)$ is important to consider as there is a bath (i.e., the substrate) to which deposited heat can escape. This heat escape, described as $T = T_0 \exp(-t/\tau_{\text{sub}})$ (where tau derives from the thermal mismatch between sample and

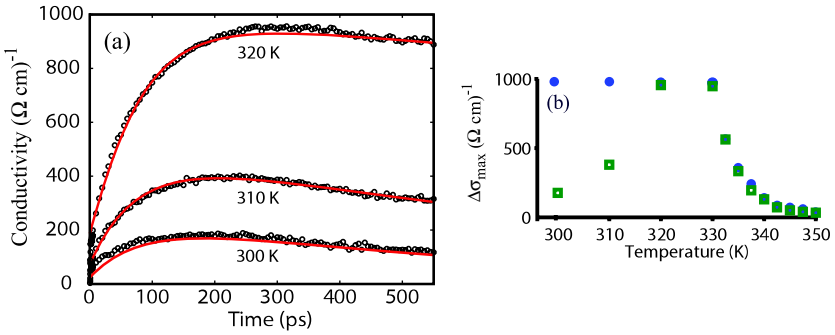

FIG. 3 (color online). (a) Induced conductivity change as a function of time at a fluence of 12.8 mJ cm^{-2} for various initial temperatures. (b) Magnitude of the induced conductivity (■) and the maximum possible conductivity change (●). The black lines are a fit as described in the text. (c) Fluence threshold as a function of base temperature.

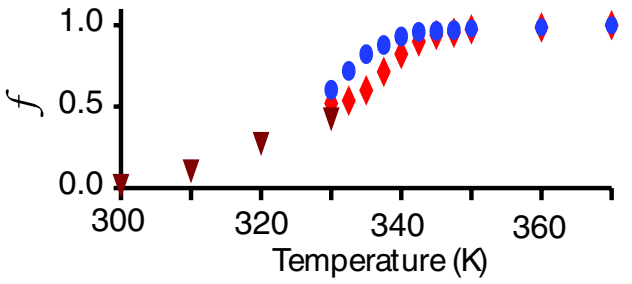

FIG. 4 (color online). The volume fraction, f_m, responsible for the observed conductivity shown in Fig. 1 (◆ for $T_\uparrow$ and ● for $T_\downarrow$) and the extracted volume fraction in the insulating state (▼) as determined from the dynamic BEMT described in the text.

substrate) imparts a time dependence to $\beta(T)$. This allows for the parametrization of $\beta(T)$ in terms of t. A subsequent Taylor expansion of β about $t = 0$ yields an analytical solution to Eq. (2) given by $f_m(t) = \Phi/(1 + \Phi)$ where $\Phi(t) = f_m^i/(1 - f_m^i)\zeta$ where f_m^i is the initial metallic volume fraction, and $\zeta = \exp\{\tau_{\text{sub}}^r \beta_0^r [1 - \exp(-t/\tau_{\text{sub}}^r)]\}$. It is the term ζ which, even in the presence of superheating well above T_c, prevents the full conductivity from being obtained. The superscript r indicates that dimensionless factors (>1) from the Taylor expansion have been incorporated into the effective lifetime and rate to simplify the expressions in this phenomenological model.

This solution describes the situation where the rate of increase of f_m decreases as energy initially deposited in the film escapes to the substrate. This determines the rise time of the conductivity and maximum induced change which in turn depends on the initial temperature (immediately after heating) and the initial volume fraction. We emphasize that this solution describes the rise time and must be multiplied by another exponential $\exp(-t/\tau_d)$ to include the subsequent conductivity decay (parametrized by τ_d). The solid lines in Fig. 3(a) are fits using this description where, for two dimensions $\sigma(t) = [2f_m(t) - 1]\sigma_m$. For the fits, $\tau_{\text{sub}}^r = 100$ ps, $\beta_0^r = 3.2 \times 10^{10}$ s^{-1}, $\tau_d = 1$ ns, and $f_m^i = 0.08$ (300 K), $f_m^i = 0.13$ (310 K), and $f_m^i = 0.3$ (320 K). The values of f_m^i in the insulating phase are plotted in Fig. 4.

We see that BEMT, appropriately extended to describe a dynamic metallic volume fraction, can account for the observed conductivity dynamics and strongly suggests a scenario where metallic precursors grow and coalesce upon photoinduced superheating. Furthermore, the results display an initial condition sensitivity described by the initial volume fraction f_m^i. We note that our analysis has assumed homogeneous growth of f_m from an initial f_m^i. It is possible that there is also photoinduced nucleation in which case the values of f_m^i will be smaller than what we have estimated from our analysis. Nonetheless, even in the case of photoinduced nucleation, the experimental data still reveal an initial condition sensitivity consistent with softening of the insulating phase and the BEMT describes the essence of the observed conductivity response.

In summary, we studied the near-threshold behavior of the photoinduced phase transition in VO_2. For the first time, we use optical pump THz-probe measurements to directly measure the change in conductivity of the system. The observed dynamics of the photoinduced phase transition result in the enhancement of fluctuations as the temperature is increased toward the transition temperature. These results may also be conducive to high-sensitivity optical devices, which make use of correlated oxides for switching, detection, or optical limiters.

We thank G. T. Wang and D. A. Yarotski for assistance with the film thickness measurements and M. Croft for an insightful discussion. This research has been supported by the Los Alamos National Laboratory Directed Research and Development program.

*Present address: Department of Physics, University of Alabama–Birmingham, 1530 3rd Ave. S., Campbell Hall 310, Birmingham, AL 35294-1170, USA.

†Present address: Department of Physics, Boston University, 590 Commomwealth Ave., Boston, MA 02215, USA. raveritt@physics.bu.edu

[1] R. D. Averitt *et al.*, J. Phys. Condens. Matter **14**, R1357 (2002).
[2] Special Topics, Photoinduced Phase Transitions and Their Dynamics, edited by S. Koshihara and M. Kuwata-Gonokami [J. Phys. Soc. Jpn. **75** 011006 (2006)].
[3] A. Cavalleri *et al.*, Phys. Rev. Lett. **87**, 237401 (2001).
[4] E. Collet *et al.*, Science **300**, 612 (2003).
[5] S. Iwai *et al.*, Phys. Rev. Lett. **91**, 057401 (2003).
[6] J. B. Goodenough, J. Solid State Chem. **3**, 490 (1971).
[7] R. M. Wentzcovitch *et al.*, Phys. Rev. Lett. **72**, 3389 (1994).
[8] A. Zylbersztejn and N. F. Mott, Phys. Rev. B **11**, 4383 (1975).
[9] I. Balberg and W. R. Roach, *Conduction in Low Mobility Materials* (World Scientific, Singapore, 1971), pp. 77–85.
[10] W. R. Roach, Appl. Phys. Lett. **19**, 453 (1971).
[11] M. Rini *et al.*, Opt. Lett. **30**, 558 (2005).
[12] A. Cavalleri *et al.*, Phys. Rev. B **70**, 161102(R) (2004).
[13] A. Cavalleri *et al.*, Phys. Rev. B **69**, 153106 (2004).
[14] A. Cavalleri *et al.*, Phys. Rev. Lett. **95**, 067405 (2005).
[15] M. Fiebig *et al.*, Science **280**, 1925 (1998).
[16] X. J. Liu *et al.*, J. Phys. Soc. Jpn. **72**, 1615 (2003).
[17] D. Brassard *et al.*, Appl. Phys. Lett. **87**, 051910 (2005).
[18] *Sensing with Terahertz Radiation*, edited by D. Mittleman, Optical Sciences Vol. 85 (Springer, Berlin, 2003), 1st ed.
[19] L. Duvillaret, F. Garet, and J.-L. Coutaz, IEEE J. Sel. Top. Quantum Electron. **2**, 739 (1996).
[20] F. J. Morin, Phys. Rev. Lett. **3**, 34 (1959).
[21] D. A. G. Bruggemann, Ann. Phys. (Leipzig) **24**, 636 (1935).
[22] D. Stroud, Phys. Rev. B **12**, 3368 (1975).
[23] H. S. Choi *et al.*, Phys. Rev. B **54**, 4621 (1996).
[24] Y. J. Chang *et al.*, Thin Solid Films **486**, 46 (2005).
[25] J. P. Sethna, *Statistical Mechanics* (Clarendon Press, Oxford, 2007), pp. 244–246.